

Glasses in hard spheres with short-range attraction

K.N. Pham, S.U. Egelhaaf, P.N. Pusey, W.C.K. Poon

School of Physics, The University of Edinburgh, Mayfield Road, Edinburgh EH9 3JZ, U.K.

(Dated: November 8, 2018)

We report a detailed experimental study of the structure and dynamics of glassy states in hard spheres with short-range attraction. The system is a suspension of nearly-hard-sphere colloidal particles and non-adsorbing linear polymer which induces a depletion attraction between the particles. Observation of crystallization reveals a re-entrant glass transition. Static light scattering shows a continuous change in the static structure factors upon increasing attraction. Dynamic light scattering results, which cover 11 orders of magnitude in time, are consistent with the existence of two distinct kinds of glasses, those dominated by inter-particle repulsion and caging, and those dominated by attraction. Samples close to the ‘A3 point’ predicted by mode coupling theory for such systems show very slow, logarithmic dynamics.

I. INTRODUCTION

Glassy states are found in many systems [1]. However, understanding the glass transition is still a major challenge for statistical and condensed-matter physics. Simple and well-characterized models hold an important place in this field. The glass transition in the simplest model colloid, a suspension of hard spheres, has been studied in detail for more than a decade [2–5]. The phase behaviour of a system of N hard-spheres of radius R in volume V is determined by a single variable, the density or volume fraction $\phi = (4/3)\pi R^3 N/V$. Increasing ϕ drives the system from a stable fluid to a fluid-crystal coexistence, and then a fully crystallized phase [2], which should be the thermodynamically favorable phase up to $\phi = \pi/3\sqrt{2} \approx 0.74$. However, at $\phi \geq \phi_g \approx 0.58$, hard spheres fail to crystallize [2, 3]. This is usually interpreted as a glass transition due to the caging of particles by each other. The most successful theoretical account given of this transition to date is from mode coupling theory (MCT) [3, 4]. Within this framework, the coupling between different density fluctuation modes drives the system into a dynamically arrested state [5].

More recently, the focus of attention has moved on to hard spheres with a short-range attraction. Besides being a good model for understanding the fundamentals of the glass transition, such ‘sticky hard spheres’ are also ubiquitous in applications. Attraction in hard-spheres can be realized experimentally by adding non-adsorbing polymers to colloids. The center of mass of a polymer coil of radius of gyration r_g is excluded from a zone of width $\sim r_g$ from the surface of each colloid. When two colloids come close enough to each other so that their polymer-excluded regions overlap, the imbalance in polymer osmotic pressure pushes them together. This effective ‘depletion’ attraction is well described [6] by the Asakura-Oosawa form [7]. Its dimensionless range can be estimated by the ratio $\xi = r_g/R$, while its strength is governed by the concentration of polymer coils in the free volume available to them, c_p^{free} . The free volume depends on the exact structure of the suspension, and is not an easily obtained experimental parameter. However, the concentration of polymer in the whole system,

c_p , can be used as an alternative variable to describe the composition of the system [8].

The presence of a short-range attraction in hard spheres widens the equilibrium fluid-crystal coexistence region in the phase diagram [8, 9], and introduces (non-equilibrium) gels at low volume fractions [10, 11] and a re-entrant glass transition at high volume fractions [12–22]. In this paper we report a comprehensive study of structure and dynamics in the vicinity of this re-entrant glass transition in a model colloid-polymer mixture: sterically-stabilized polymethylmethacrylate particles with added linear polystyrene [23].

We used light scattering to study the structure of colloids by measuring the static structure factor (SSF), $S(q)$, which is effectively the Fourier transform of the pair correlation function. Dynamic light scattering was used to obtain the normalized collective dynamic structure factor (DSF), $f(q, \tau)$, which measures the time correlation of particle density fluctuations at wave vector q after delay time τ . Our results agree in broad outline with previous experimental studies and the trends predicted by MCT, while the detailed nature of our study and the very wide time window of our measured DSFs (11 orders of magnitude) together shed new light on the nature of the re-entrant glass transition in sticky hard spheres. Preliminary reports of some of these data have been given before [17, 24].

II. EXPERIMENTAL METHODS

A. Sample preparation

The colloidal particles used in this study were polymethylmethacrylate (PMMA) spheres sterically stabilized by chemically-grafted poly-(12-hydroxystearic acid) (PHSA) dispersed in *cis*-decalin [25]. The solvated PHSA, approximately 10nm thick, produces a nearly-hard-sphere interaction between the colloidal particles [26]. The particle radius, $R = 202\text{nm}$, was determined from the lattice spacing of the crystal phase at fluid-crystal coexistence, taking the crystal to be at $\phi = 0.545$. Particle size polydispersity was 0.069, measured from the

apparent angle dependence of the diffusion coefficient in a dilute suspension [27].

The colloidal volume fraction was calibrated by measuring the amount of crystal phase in the coexistence region and taking the fluid and crystal volume fraction to be at 0.494 and 0.545 respectively. Samples of the volume-fraction-calibrated stock were also weighed and dried in a vacuum oven to determine the effective density of the particles, which was then used in subsequent calculations of the volume fraction of samples prepared from the stock. The stock volume fraction was also recalibrated from time to time by drying and weighing.

To induce attraction between the colloids, we added non-adsorbing linear polystyrene. This well-characterized model colloid-polymer mixture has been studied extensively over the last decade [23]. The polymer used was purchased from Polymer Laboratories and had a molecular weight of $M_w = 370000$ daltons. Its radius of gyration in *cis*-decalin at 20°C was calculated from the data in [28] to be $r_g = 17.8$ nm. Thus the dimensionless range of the depletion attraction is $\xi \sim r_g/R = 0.09$.

Colloid-polymer mixture samples were prepared by mixing stocks of colloids and polymers with known concentration and solvent by weight. Sample volumes were about 1 cm³. Knowing the density of each species permits calculation of the final composition.

The main uncertainty in sample composition comes from a systematic uncertainty in the calibrated volume fraction of the colloid stock. This is because the volume fractions of coexisting fluid and crystal phases for slightly polydisperse hard-spheres are slightly different from those in a monodisperse colloid, but the exact values are uncertain [29, 30]. However, all samples were prepared from the same stocks of colloids and polymer solutions, or stocks calibrated against each other. Some samples were also derived from others in a controlled way (see next paragraph). Therefore despite some systematic uncertainties in the estimation of absolute volume fractions due to polydispersity, the uncertainties in sample compositions relative to each other were mostly from random errors in weighing. These uncertainties are below a percent in the worst case and are insignificant in this work.

Samples were tumbled for prolonged periods of time to ensure proper mixing of the components. After homogenizing, a small amount of each sample was transferred to 3 mm-inner diameter glass tubes and sealed for light scattering experiments. The rest of the sample was then left undisturbed for visual observation of any phase transitions until sedimentation appeared. Then some samples may be diluted with solvent while others were left opened for solvent to evaporate before re-homogenizing. In this way, a sequence of samples, some very close in composition, could be prepared.

B. Light scattering methods

The slight difference in the refractive indices of PMMA and *cis*-decalin (1.49 and 1.48 respectively) was enough to render all of our samples turbid (transmission coefficients ≈ 20 –40%). We therefore used two-color light scattering to extract the singly-scattered component. The detailed experimental arrangement and data analysis for this method have been described elsewhere [31]. Here we just summarize relevant procedures.

Two lasers of different wavelengths, blue ($\lambda_B = 488$ nm) and green ($\lambda_G = 514.5$ nm), and two detectors with filters were used in what were essentially two separate but simultaneous scattering experiments on the same scattering volume. The incident and scattered beams were arranged such that the scattering angles θ_B and θ_G were different but the scattering vectors were identical, i.e. $\mathbf{q}_B = \mathbf{q}_G = \mathbf{q}$, where $|\mathbf{q}| = 4n\pi \sin(\theta/2)/\lambda$ and n is the refractive index of *cis*-decalin. The outputs of the two detectors were cross-correlated to give the intensity correlation function (ICF):

$$g^{(2)}(q, \tau) = \frac{\langle I_B(q, 0)I_G(q, \tau) \rangle}{\langle I_B(q) \rangle \langle I_G(q) \rangle}, \quad (1)$$

where I_B and I_G are the scattered blue and green intensities respectively, and the angled brackets denote ensemble averages.

In this arrangement, it can be shown [31] that only the singly-scattered light of each color probes exactly the same Fourier component of the density fluctuations and thus are correlated. All other, multiply-scattered, light does not probe the same component for both colors and is completely uncorrelated and thus does not contribute to the time-dependence of $g^{(2)}(q, \tau)$. This can be expressed [31] in terms of the normalized single scattering dynamic structure factor, $f(q, \tau)$:

$$g^{(2)}(q, \tau) = 1 + \beta^2 \beta_{MS}^2 [f(q, \tau)]^2, \quad (2)$$

where the factor β^2 depends on the ratio of detector area and coherence area for single scattering and also on the overlap of the scattering volumes probed by each color. This factor is instrument related and dependent on scattering angle but not on the sample used. The other factor β_{MS}^2 reflects the fraction of singly-scattered intensities, $\langle I_B^S \rangle$ and $\langle I_G^S \rangle$, relative to the total (singly and multiply) scattered intensities:

$$\beta_{MS}^2 = \frac{\langle I_B^S \rangle \langle I_G^S \rangle}{\langle I_B \rangle \langle I_G \rangle}. \quad (3)$$

The concentration of polymer in our samples is low. The highest ratio of intensity scattered from polymer to that from colloid was measured to be 4×10^{-3} . This highest ratio only applied for one sample (H in Fig. 1) at the lowest scattering angle. Therefore we assume that the scattered intensity is from colloids only. Under these conditions, our measurements probe the structure and dynamics of the particles alone.

The static structure factor was measured with the procedure described in [32]. First, the total average intensities, $\langle I_B \rangle$ and $\langle I_G \rangle$, and the intercept, $\beta^2 \beta_{MS}^2 = g^{(2)}(q, 0) - 1$, of a concentrated sample of interest were measured at different scattering vectors q . The sample was rotated continuously during the measurement to ensure ensemble average. Since the rotation only changes the time-dependence of $g^{(2)}(q, \tau)$, the intercept and average intensity were not affected. It was found that it was necessary to average measurements at different height in the sample for non-ergodic samples to reduce random noise from the finite number of speckles sampled. Then the same measurements were made on a dilute suspension of known ϕ to obtain the single-particle form factor. The volume fraction of this dilute sample was $\phi_{dil} = 0.01$, small enough that multiple scattering can be ignored, so that the measured intercept contains only the instrument related factor: $\beta^2 = g_{dil}^{(2)}(q, 0) - 1$, which was the same as that in the measurement of the concentrated sample.

The static structure factor is the ratio of singly-scattered intensity per particle from the concentrated sample to that from the dilute sample: $S(q) = (\langle I^S \rangle / \phi) / (\langle I_{dil} \rangle / \phi_{dil})$. This was calculated by taking into account multiple scattering and attenuation of light through the sample:

$$S(q) = \frac{\phi_{dil}}{\phi} \frac{\sqrt{T_{B,dil} T_{G,dil}}}{\sqrt{T_B T_G}} \frac{\sqrt{\langle I_B \rangle \langle I_G \rangle \beta^2 \beta_{MS}^2}}{\sqrt{\langle I_{B,dil} \rangle \langle I_{G,dil} \rangle \beta^2}}, \quad (4)$$

where T is the transmission coefficient of the sample, and subscripts B, G are for blue and green light respectively.

Dynamic light scattering aims to measure the dynamic structure factor (DSF), $f(q, \tau)$. This can be extracted from normalizing the ICF using Eq. 2:

$$f(q, \tau) = \sqrt{\frac{g^{(2)}(q, \tau) - 1}{g^{(2)}(q, 0) - 1}}. \quad (5)$$

However, since most of our samples were either non-ergodic or had very slow relaxation times, the time-averaged ICF only measured fluctuations in a small subspace of the whole configuration space. Explicit ensemble averaging was therefore required, and was performed by two methods. For short times (10^{-7} s $< \tau < 20$ s), brute-force ensemble averaging was done. Several hundred (typically between 500-865) of time-averaged ICF's, $g_t^{(2)}(q, \tau)$, and associated scattered intensities, I_{Bt} and I_{Gt} , were measured, each for a duration of 40-60 s. Between each measurement, the sample was rotated by a small angle to a different position so that each time-averaged ICF sampled a different Fourier component. The ensemble-averaged ICF was then constructed as:

$$g^{(2)}(q, \tau) = \frac{\langle I_{Bt} I_{Gt} g_t^{(2)}(q, \tau) \rangle}{\langle I_{Bt} \rangle \langle I_{Gt} \rangle}. \quad (6)$$

For longer times ($\tau > 1$ s), echo DLS was used. Details will be given elsewhere [33]. It essentially involves ensemble averaging by rotating the sample continuously at

a constant speed and correlating the intensities at a small range of delay times around exact multiples, $\tau \approx nT$, of the rotation period, T , where the correlation function shows 'echo' peaks. The rotation decorrelates the ICF very quickly at small τ . However, after a whole number of revolutions, the sample comes back to the same orientation and the ICF recovers to a value that is dependent only on the dynamics of the particles in the sample over that period of time. This gives rise to peaks in the ICF at $\tau = nT$. The maxima of these peaks follow the ensemble-averaged dynamics of the sample because the obtained ICF is an average over thousands of independent speckles per revolution. We also correct for imperfections in the rotation using the area under each echo instead of the echo maximum [33]. The corrected ICF at $\tau_n = nT$ was calculated from the measured ICF $g_m^{(2)}(q, \tau)$ as:

$$g^{(2)}(q, \tau_n) = \frac{A(\tau_n)}{A(\tau_0)} [g_m^{(2)}(q, 0) - 1] + 1, \quad (7)$$

where $A(\tau_n)$ is the area under the echo around $\tau_n = nT$, $A(\tau_n) = \int (g_m^{(2)}(q, \tau) - 1) d\tau$. The DSF was then obtained from corrected ICF in the usual way from Eq. 5.

We used echo DLS to measure dynamics in the range $\tau = 1 - 10^4$ seconds. Since the rotation used introduces slightly different alignment in the DLS setup (hence different β^2), the resulting intercepts are different from those obtained by brute-force ensemble averaging. Therefore we scaled the intercept of the echo DLS results by an arbitrary factor (in the range of 1-2) so that the resulting DSF from both methods matched in the region of overlap.

III. RESULTS AND DISCUSSION

A. Phase diagram

The equilibrium phase diagrams of colloid-polymer mixtures at different values of ξ are well known [9]. The non-equilibrium behavior of systems with $\xi \approx 0.1$ at low volume fractions ($\phi < 0.2$) has been studied before [10, 11]. Here we concentrate on the higher volume fraction region ($\phi \geq 0.3$).

Many samples were prepared in a range of compositions of interest. After being homogenized by prolonged tumbling, samples were left undisturbed for observation. Because the sizes of colloidal particles are similar to wavelengths of visible light, colloidal crystals can be seen with the naked eye as iridescent specks.

Our observations are shown in Fig. 1. (These observations have been presented and briefly discussed before [24].) In agreement with equilibrium theory [8] for systems with short-range attraction, we observed an expansion of the fluid-crystal coexistence region upon increasing polymer concentration (diamonds). To the left of this region is a stable fluid phase (triangles) and to the right is the fully crystalline phase (inverted triangles).

These observations also agree with previous experiments on similar systems [9].

However, samples with very high colloid volume fractions and/or polymer concentrations (filled circles, squares and crosses) failed to crystallize for weeks to months even though equilibrium statistical mechanics predicts either fluid-crystal coexistence or full crystallinity. Samples with high colloid volume fractions and low polymer concentrations (circles in Fig. 1) showed all the characteristics of hard-sphere colloidal glass [2]. Weeks after homogenization and left undisturbed, sedimentation showed its effect: very thin layers at the top of the samples developed heterogeneous crystals due to the boundary effect of the meniscus and gravity. Samples denoted by squares in Fig. 1, with high polymer concentration and moderate colloid volume fraction, showed signs of transient gels. They collapse under gravity after some ‘latency time’ as observed previously in similar systems [10, 11]. However, the amount of collapse decreased and transient time increased dramatically in higher volume fraction samples. For concentrated samples with colloid volume fraction above 0.55, it took more than 4 weeks to see tiny collapses of less than half a millimeter at the very top of the meniscus. These collapses were distinguished from normal sedimentation by their characteristic sharp and non-flat boundary between the collapsed material and a clear supernatant. No crystallization was observed in these samples however long they were left undisturbed. Interestingly, for non-crystallizing samples with very high colloid volume fraction and polymer concentration (crosses), characteristics of both hard-sphere glass and transient gels were present. After 4–8 weeks, tiny collapses were seen, and also a thin layer of crystal phase appeared just under the collapsing boundary.

Consider a sequence of samples of similar colloid volume fraction and increasing attraction, for example samples A–H in Fig. 1 with $\phi \sim 0.6$. According to thermodynamic equilibrium theory, all these samples should crystallize [8]. Sample A without polymer was a glass. Sample B with a small amount of polymer was also a glass as no homogeneous crystallization was observed for 4 weeks and only heterogeneously nucleated crystals at the meniscus were observed after 13 days. However, sample C with $\sim 1.4 \text{ mg cm}^{-1}$ of polymer completely crystallized in 1 day. This means the glass transition line has moved to higher ϕ . Failure to crystallize was seen again for samples with polymer concentration above $\sim 2.5 \text{ mg cm}^{-1}$ (samples F,G,H). The behavior of all the samples in this region taken together show that the line of failure to crystallize had a re-entrant shape.

In pure hard-spheres, crystallization ceases at essentially the same volume fraction as where $f(q, \infty)$ first becomes non-zero, i.e. at the glass transition [2, 3]. If this coincidence still holds for attractive hard-spheres systems, then we have observed a re-entrant glass transition in hard spheres with short-range attraction.

Previous studies of sticky hard spheres by MCT [16, 20] and computer simulation [17, 18] suggest that the re-

entrant behavior is due to two different mechanisms of glassy arrest. The heuristic picture is as follows. In the ‘repulsion-dominated’ hard-sphere glass, particles are caged by their neighbors at high enough volume fraction. Short-range attraction clusters the particles of the cage and opens up holes, ultimately melting the glass. However, increasing the attraction further leads to an ‘attraction-dominated’ glass where particles stick to their neighbors with long-lived bonds. In this terminology, samples A and B are repulsive glasses and F–H are attractive glasses. Samples I–K must lie in the region where these two types of glass merge as they show characteristics of both types, with further evidence in the dynamics shown in section III C. The next sections, with results from light scattering, will give insights into the structure and dynamics of these glasses, and the nature of the re-entrant transition between them.

B. Static structure factor

We measured the static SSFs of the samples whose symbols are circled in Fig. 1. Note that samples C–E were measured as metastable fluids, i.e. before any crystal nucleation took place. Consider first the results for a sequence of samples (A–H) with $\phi \approx 0.6$, Fig. 2. These samples span the re-entrant glass transition line where the crystallization behavior showed dramatic changes. However, no re-entrant behavior can be seen in the SSF. Instead, there are only gradual changes upon increasing the attractive interaction. These gradual changes have been predicted by theory [16], and observed before in other experimental systems [34].

The most obvious and most easily quantifiable changes are in the height and position of the main peak. Broadly speaking, and taking experimental uncertainties into account, the peak reduces in height and shifts to higher q when the attraction is increased (inset Fig. 2(a)). In detail, the peak position, q^* , remains constant (at $q^*R \approx 3.8$, samples A–D) until just before we enter the attractive glass region (sample E), whereupon it increases by $\approx 5\%$ to reach another constant value ($q^*R \approx 4$, samples F–H). These samples have approximately constant ϕ (in fact it decreases slightly from A to H, Fig. 1). The increase in q^* is the result of a significant fraction of neighboring particles becoming trapped in each others’ narrow depletion potential well when the attractive glass forms. Quantitatively, a 5% increase in q^* corresponds to a 15% increase in the local packing fraction, from 0.6 to 0.69; the latter is the random close packing volume fraction for our system (measured by spinning down a sample of known ϕ). In other words, the nearest particles in the attractive glass are practically touching.

The clustering of particles at constant volume necessarily implies that the average number of nearest neighbors should decrease, and that ‘holes’ are opened up to render the structure more inhomogeneous on the spatial scale of a few particles. The former is reflected in the decrease in

$S(q^*)$. Significantly, upon increasing the attraction from zero, the decrease in the peak height starts at the point of the melting of the repulsive glass, and continues until we enter the attractive glass region, whereupon the peak height remains constant (inset Fig. 2(a)).

The increased heterogeneity is reflected in a rise in the SSF at low q , Fig. 2(b). The smallest q we have studied was $q_{\min}R = 1.50$, corresponding to a length scale of about 4 particle radii. The value of $S(q_{\min})$ increases nearly exponentially with the polymer concentration between samples A–E (inset Fig. 2(b)), and thereafter remains constant. The increased density fluctuations at this length scale corresponds to the opening up of ‘holes’ due to particle clustering.

Note that all three features considered, q^* , $S(q^*)$ and $S(q_{\min})$, remain virtually constant for all three attractive glass samples, F–H. Once particles drop into each others’ narrow attractive potential wells, any further *structural* changes will be hard to resolve. We shall see, however, that the *dynamics* continues measurably to evolve from sample F to sample H: in this regime of almost-touching nearest neighbors, a very small change in the structure has very large dynamic consequences.

All the qualitative features we observed in the evolution of the SSFs for samples A–H are also seen in the SSFs for samples I–K at the higher volume fraction of $\phi \approx 0.64$, Fig. 3. However, the effects are significantly less obvious, largely because the range of polymer concentration is now much smaller and ϕ is higher. At low q , the values of $S(q_{\min})$ are lower than those of similar polymer concentration but lower ϕ (C–E) (Fig. 2(b)). This is because at higher volume fraction, a tight local clustering of some particles does not create so much room elsewhere — there is less space for developing heterogeneities.

C. Dynamic structure factor

Our goal is to study how the polymer-induced depletion attraction affects the particle dynamics. But the presence of the polymer influences the dynamics in another, essentially trivial, manner — by increasing the effective viscosity of the medium in which the particles diffuse from that of the pure solvent, η_0 , to that of a polymer solution, $\eta_r\eta_0$ at concentration c_p^{free} . To determine η_r , we measured the viscosity of pure polymer solutions with a miniature suspended-level viscometer, Fig. 4, and used a quadratic fit to the data to obtain η_r for our samples. The value of c_p^{free} in each sample was estimated from c_p , ϕ and ξ using an approximate expression based on scaled-particle theory [8].

The rate of dynamical decay at wave vector q depends on the length scale being probed; in dilute systems it scales as q^2 . Thus, in order to compare the dynamics of different samples at different wave vectors, and to highlight the effects of the attraction, we scaled the delay time variable of the DSFs by the relative viscosity η_r and the dimensionless wave vector $(qR)^2$, so that DSF is pre-

sented as a function of the ‘scaled time’ $(qR)^2\tau/\eta_r$. Note that for the lowest q studied, the scaled time is very close to the real time, while at the highest q , it is increased by about an order of magnitude.

We found aging [35] in all non-crystallizing samples. The dynamics slowed down with the ‘waiting time’ — the time interval between the cessation of tumbling and the beginning of measurements, Fig. 5. It is known that the hard-sphere glass ages [36]. We found that the rate of aging in different glasses were different and that its effects were complex. Repulsive glasses aged only in the first day or two, after which they did not evolve within the time window of the measurements. Attractive glasses, on the other hand, showed different dynamics with age for up to 10 days. Aging is complicated enough to be the subject of a separate study and was not investigated systematically in this work. To eliminate as much as possible aging effects on dynamical results within practical limits of waiting time, we present DSFs of glassy samples with age between 1 and 4 days. The dynamics of crystallizing samples (C–E) were measured while they were in the metastable state well before the appearance of crystallization. Below we first show results of different samples at the same q , then at different q for the same sample.

1. Constant scattering vectors, variable compositions

The DSFs of samples A–H at $qR = 1.50$, Fig. 6, clearly evolve non-monotonically with increasing polymer concentration and show re-entrant behavior. Briefly, samples A and B are non-ergodic within our time window, while samples C–E are ergodic (their DSFs decay completely to zero), and samples F–G become non-ergodic again.

In detail, the DSF of sample A, a pure hard-sphere glass, shows a plateau at $f_A(q, \infty) \approx 0.7$, corresponding to particles getting ‘stuck’ in their nearest-neighbor cages. This can be compared with previous work [3, 37]. Note that in doing so, it is important to compare samples with the same density *relative to random close packing*: i.e. the same $(\phi_{\text{rcp}} - \phi)/\phi_{\text{rcp}}$, since ϕ_{rcp} differs according to the polydispersity of the colloids [38].

With a small amount of polymer added to the hard-sphere glass, sample B shows the same qualitative dynamics. Quantitatively, however, the height of the plateau is lower, $f(q, \infty) = 0.62$. This indicates that particles in B are not as restricted as in A, i.e. the cage is loosened by the attractive interaction, but still remains closed in our time window.

The DSF of sample C decayed completely in (a ‘scaled time’ of) about 1000 seconds, as did those for the other crystallizing samples D and E. It is interesting to note that the DSFs of these three samples slow down upon increasing polymer concentration but all reach zero at about the same scaled time. The DSF of sample C shows the remnant of a plateau at a scaled time of ≈ 10 s. The DSFs for samples D and E exhibit a very stretched *single*

decay, rather than a two-stepped process. This is unusual behavior for a fluid at volume fraction $\phi \sim 0.6$ (at least at first sight).

The intermediate, β , and long-time, α , decay in a dense hard-sphere fluid are attributed to particles ‘rattling’ in their local neighbor cages, and escaping from these cages, respectively [3]. Attraction hinders the ‘rattling’ by trapping particles in potential wells, but accelerates the cage opening by clustering. At some polymer concentration (or attraction strength), the two time scales coincide. If at this point the attraction alone is not enough to trap the system in a non-ergodic state, we will observe the melting of the repulsive glass into an ergodic fluid dominated by attraction. This is the case for sample C, where the α and β decays are barely distinguishable in the DSF. At higher polymer concentrations, the cage concept is no longer appropriate for describing the particle dynamics — for it to be valid, a particle has to ‘rattle’ many times in a cage before it opens. Note that this is a distinctive feature of dense fluids with *short-range* attraction. In a dense fluid with *long-range* attraction, the effective potential well experienced by any particle due to its neighbors is essentially flat. This adds a (negative) constant to the free energy, so the phase behavior [39] and dynamics of the system are still controlled by repulsion (or, equivalently, entropy).

Note that the shape of the DSF of sample C at $qR = 1.50$ is similar to that shown in curve 2, Fig. 11 of [16]. This DSF was calculated at $qR = 2.1$ for a sample in the re-entrant portion of the state diagram in a system that *just* shows a glass-glass transition and an A3 point. Recent calculations for colloid-polymer mixtures [20] suggests that our system, with $\xi \approx 0.09$, should show exactly these features.

The DSFs of samples F–H are, once more, non-ergodic in our time window: they do not decay completely even after 10^4 seconds. Simple extrapolation indicates that it would take these DSFs at least 10^6 seconds to reach zero. The DSFs of samples G and H show points of inflection; that for sample H is clearer and occurs at $f = 0.995$ — a very high value compared to the plateaus in hard-sphere glasses. These high points of inflection can be associated with dynamics originating from particles rattling in very narrow attractive potential wells.

At other wave vectors, Figs. 7 and 8, the DSFs behave in a similar way, namely relatively low plateaus in the repulsive glasses A and B, complete decay in the metastable fluids C–E, and extremely slow dynamics in the attractive glasses F–H, with very high points of inflection in G and H. Note, however, that at the peak of the corresponding SSFs, the DSFs for samples C–E are barely distinguishable (Fig. 7).

The plateaus in the DSFs of the repulsive glasses can be used as a measure of $f(q, \infty)$, the non-ergodicity parameter. An estimate of this quantity for the attractive glasses is more problematic, partly due to significant aging in our time window. To proceed, we use the value of f at the point of inflection as a surrogate; we call this

the ‘measured’ $f(q, \infty) \equiv f^{(M)}(q, \infty)$. The evolution of $f^{(M)}(q, \infty)$ with increasing polymer concentration (samples A–H) is shown in Fig. 9. The non-ergodicity parameter decreases slightly when moving from A to B, away from the hard-sphere glass. When attraction melts the repulsive glass, $f^{(M)}(q, \infty) = 0$ for samples C–E (not shown). Sample F did not crystallize and showed non-ergodic dynamics up to 10^4 seconds but did not exhibit any discernible point of inflection in its dynamics. Samples G and H had extremely high non-ergodicity parameters of nearly 1. A ‘jump’ in $f(q, \infty)$ when moving from repulsive to attractive glass was predicted by MCT (Fig. 7 in [16]).

The evolution of the short-time dynamics of the whole sequence of samples is also interesting. Fig. 10 shows the short-time behavior of the DSFs for A–H at large length scale, $qR = 1.50$, where experimental noise is lowest. Note the very small vertical interval, 1.000 to 0.997, spanned in this figure; thus only the first 0.3% of the decays of the DSFs are being analyzed. The DSFs of repulsive glasses A and B possessed relatively long linear parts, corresponding to the first term in τ in the expression derived from the Smoluchowski (many-particle diffusion) equation [40]: $f(q, \tau) = 1 - \frac{D_0 H(q)}{\eta_r S(q)} q^2 \tau + O(\tau^2)$, where D_0 is the free-particle diffusion constant in pure solvent (with no polymer) $D_0 = k_B T / 6\pi\eta_0 R$, and $H(q)$ is the hydrodynamic factor. This linear regime of the DSFs indicates that at short time, individual particles still diffuse freely without the influence from direct interaction with their neighbors. The change in limiting slope as $\tau \rightarrow 0$, or the short-time diffusion coefficient $D_s(q) = D_0 H(q) / S(q)$, can be almost entirely explained by the change in $S(q)$ (Fig. 11), including the strong decrease on entering the attractive glass regime. What is more interesting is that the dynamics depart from free diffusion progressively earlier upon increasing attraction (Fig. 10). In fact, for the attractive glasses F–H, the particles are confined so tightly by the attractive potential wells that the DSFs display non-linearity almost immediately (cf. also insets to Figs. 6–8).

Moving to the (shorter) sequence of samples at the higher volume fraction of $\phi \approx 0.64$ and closer to the intersection of the two glass transition lines, samples I–K in Fig. 1, we see the emergence of remarkably stretched-out, extremely slow dynamics. Consider first the data at $qR = 1.50$, Fig. 12. In terms of short-time dynamics (inset, Fig. 12), samples I and J are comparable to samples C and D, while sample K shows a behavior intermediate between those of samples E and F. At intermediate times, the decay is linear with respect to the logarithm of the scaled time. Thereafter there is an incipient plateau at $f \sim 0.7$ in sample I, reminiscent of the plateau in repulsive glasses A and B, before a further decay, but never beyond ~ 0.62 in our time window. There is no incipient plateau for the other two samples. Note that the DSF of sample I shows aspects of the behavior of repulsion-dominated glasses (long time) and a fluid dominated by short-range attraction (short time). The two regimes are

‘bridged’ by a stretched log-time decay.

At the peak of the SSF, Fig. 13, sample I behaves in a similar way at short to intermediate times, while there is no incipient plateau at long times. Samples J and K develop an incipient plateau as high as ~ 0.993 (inset Fig. 13) before turning over to decay more rapidly in logarithmic time.

The fact that these samples show extremely stretched out dynamics, logarithmic in time, suggests that they are very close to the A3 critical point predicted by MCT, where the repulsive and attractive glasses become indistinguishable [14, 16, 21]. In particular, the shape of the DSF of sample I at $qR = 1.5$ is comparable to curve 3 in Fig. 11 of [16], calculated at $qR = 2.1$ for a sample on the repulsive glass transition line very close to where it intersects the attractive glass transition line for a system that just shows an A3 singularity. This is not inconsistent with the position of sample I on the state diagram, Fig. 1, of our system at $\xi \approx 0.09$ [20].

Heuristically, we may begin to make sense of log-time decays as follows. At high enough volume fraction, the average distance between neighboring particles will decrease to a value such that they are always well within the attraction range of each other [41]. If the attraction is strong enough, the restriction of particle movement due to the neighbor cage and the restriction caused by bonding between particles take place simultaneously at all times. This competition between two opposite mechanisms may lead to a broad distribution of decay times and therefore a very stretched out DSF [42].

2. Constant compositions, variable scattering vectors

In this section, we show for completeness the dynamics of each sample at different scattering vectors in Figs. 14–17. The change of DSFs with q in repulsive glasses A and B are in agreement with previous work [3, 37]. Other samples show the general trend that the dynamics become slower at scattering vectors with higher $S(q)$. The only exception concerns the intermediate-time dynamics of the attractive glasses F–H (insets, Fig. 16). The significance of the rather complicated q -dependence of the intermediate-time dynamics of these samples is not clear. Nor do we know of any detailed calculations to date that can throw light on this issue.

The systematic q -dependent data shown in Figs. 14–17 allow us to investigate the q -dependence of the measured non-ergodicity parameter, $f^{(M)}(q, \infty)$, in detail. The measured non-ergodicity parameters of glassy samples A, B, G and H are shown as a function of scattering vector q in Fig. 18. The data for repulsive glasses A and B vary essentially with the static structure factor, as observed in hard-sphere glasses [37]. Attractive glass G and H on the other hand showed extremely high measured non-ergodicity parameters that hardly vary with q . This agrees with predictions by MCT (c.f. Fig. 8 in [16]).

IV. CONCLUSION

We have studied a dense system of hard-sphere colloids with a short-range inter-particle attraction induced by the depletion effect of added non-adsorbing polymer. The observed crystallization behavior as well as particle dynamics studied by DLS reveal a re-entrant glass transition. With little attraction, the system at high enough volume fraction is ‘stuck’ in a repulsive glassy state where the arrest is due to caging by neighboring particles. Our data support the suggestion [13] that attraction causes particles to cluster, thus opening up holes in the cages and melting the glass. At the same time, the attraction slows down the particle dynamics. We found that the repulsive glass melts when the characteristic time of the attraction-dominated particle dynamics becomes comparable to that of cage opening. The resulting ergodic fluid shows a distinctive dynamical feature: despite the fluid’s high density, its DSF does not show distinct α and β relaxation processes. Increasing the attraction further leads to different kind of arrest where the strong attraction between particles create long-lived bonds and prevent structural rearrangement, giving rise to an attraction-dominated glass. Detailed light scattering has been used to probe the effect of attraction on both structure and dynamics.

Qualitatively, this scenario agrees well with predictions from MCT calculations (with those reported in [20] being closest to the present experimental system). In particular, we observed very slow, log-time dynamics in the DSFs in the region where the two glass transition lines are expected to meet. Quantitatively, however, our results stand as a challenge to MCT (or any other theory): the detailed calculations needed for direct quantitative comparison have not, to our knowledge, been performed.

A detailed comparison between experiment and theory faces a number of non-trivial problems. First and foremost, since calculated and measured glass transition thresholds differ, choices exist as to what constitute ‘corresponding state points’ for the purpose of making the comparison. In the case of pure hard spheres, where $\phi_g^{\text{MCT}} \approx 0.52$ and $\phi_g^{\text{expt}} \approx 0.58$, it is accepted practice to compare measurements and calculations at the same relative volume fraction $(\phi - \phi_g)/\phi_g$ [3]. The situation is more complex in a colloid-polymer mixture, since a state point is now specified by the densities of both components. The predicted glass transition lines show quantitative disagreement with experiments over the whole composition plane (cf. Fig. 1 in [17]). To compare calculated and measured SSFs and DSFs, a protocol for identifying ‘corresponding state points’ is needed.

Secondly, the attractive interaction between two particles is always specified directly as a potential energy in calculations. The corresponding experimental variable is the polymer concentration in the free volume, c_p^{free} . This is currently guessed at using an uncontrolled and untested approximation based on scaled-particle theory [8], and is likely to lead to large systematic errors in sys-

tems with high colloid volume fractions. Thirdly, the marked and complex aging behavior of the attractive glasses complicates the definition of a non-ergodic state for the purposes of comparing with MCT. Despite these potential difficulties, however, our data suggest that it may be worthwhile performing a series of calculations at fixed ϕ and increasing attraction crossing the re-entrant gap in between the repulsive and attractive glass transition lines for a system of hard spheres interacting with something like an Asakura-Oosawa potential [20].

Finally, it is clear that attractive and repulsive glasses show qualitative distinct aging behavior. Classical MCT does not predict aging, but it is a generic feature of experimental glasses of all kinds [35]. A number of theoretical approaches are emerging, and simulation is a valuable tool. It is probable that further study of this phe-

nomenon in our model colloid-polymer mixture should throw significant light on this intriguing (and generic) phenomenon [22].

Acknowledgments

KNP is funded by an UK ORS award and the University of Edinburgh. Partial financial support for experimental equipment came from EPSRC grant GR/M92560. We thank Matthias Fuchs, Michael Cates, Antonio Puer-tas, Johan Bergholtz and Francesco Sciortino for illuminating discussions during various stages of this work, and Michael Cates also for commenting on the manuscript.

-
- [1] C. A. Angell, *Science* **267**, 1924 (1995).
 - [2] P. N. Pusey and W. van Meegen, *Nature* **320**, 340 (1986).
 - [3] W. van Meegen and S. M. Underwood, *Phys. Rev. E* **49**, 4206 (1994).
 - [4] U. Bengtzelius, W. Götze, and A. Sjölander, *J. Phys. C* **17**, 5915 (1984).
 - [5] W. Götze and L. Sjogren, *Rep. Prog. Phys.* **55**, 241 (1992).
 - [6] D. Rudhardt, C. Bechinger, and P. Leiderer, *Phys. Rev. Lett.* **81**, 1330 (1998).
 - [7] S. Asakura and F. Oosawa, *J. Chem. Phys.* **22**, 1255 (1954).
 - [8] H. N. W. Lekkerkerker, W. C. K. Poon, P. N. Pusey, A. Stroobants, and P. B. Warren, *Europhys. Lett.* **20**, 559 (1992).
 - [9] S. M. Ilett, A. Orrock, W. C. K. Poon, and P. N. Pusey, *Phys. Rev. E* **51**, 1344 (1995).
 - [10] W. C. K. Poon, A. D. Pirie, and P. N. Pusey, *Faraday Discuss.* **101**, 65 (1995).
 - [11] W. C. K. Poon, L. Starrs, S. P. Meeker, A. Moussaïd, R. M. L. Evans, P. N. Pusey, and M. M. Robins, *Faraday Discuss.* **112**, 143 (1999).
 - [12] J. Bergholtz and M. Fuchs, *J. Phys.: Condens. Matter* **11**, 10171 (1999).
 - [13] J. Bergholtz and M. Fuchs, *Phys. Rev. E* **59**, 5706 (1999).
 - [14] L. Fabbian, W. Götze, F. Sciortino, P. Tartaglia, and F. Thiery, *Phys. Rev. E* **59**, R1347 (1999).
 - [15] F. Mallamace, P. Gambadauro, N. Micali, P. Tartaglia, C. Liao, and S.-H. Chen, *Phys. Rev. Lett.* **84**, 5431 (2000).
 - [16] K. Dawson, G. Foffi, M. Fuchs, W. Götze, F. Sciortino, M. Sperl, P. Tartaglia, T. Voigtmann, and E. Zaccarelli, *Phys. Rev. E* **63**, 011401 (2001).
 - [17] K. N. Pham, A. M. Puertas, J. Bergholtz, S. U. Egelhaaf, A. Moussaïd, P. N. Pusey, A. B. Schofield, M. E. Cates, M. Fuchs, and W. C. K. Poon, *Science* **296**, 104 (2002).
 - [18] A. Puertas, M. Fuchs, and M. E. Cates, *Phys. Rev. Lett.* **88**, 098301 (2002).
 - [19] T. Eckert and E. Bartsch, *Phys. Rev. Lett.* **89**, 125701 (2002).
 - [20] J. Bergholtz, W. C. K. Poon, and M. Fuchs, *Langmuir* **19**, 4493 (2003).
 - [21] F. Sciortino, P. Targaglia, and E. Zaccarelli, preprint, cond-mat/0304100.
 - [22] E. Zaccarelli, G. Foffi, F. Sciortino, and P. Tartaglia, preprint, cond-mat/0304192.
 - [23] W. C. K. Poon, *J. Phys.: Condens. Matter* **14**, R859 (2002).
 - [24] W. C. K. Poon, K. N. Pham, S. U. Egelhaaf, and P. N. Pusey, *J. Phys.: Condens. Matter* **15**, S269 (2003).
 - [25] L. Antl, J. W. Goodwin, R. D. Hill, R. H. Ottewill, S. M. Owens, S. Papworth, and J. W. Waters, *Colloids Surf.* **17**, 67 (1986).
 - [26] S. Auer, W. C. K. Poon, and D. Frenkel, *Phys. Rev. E* **67**, 020401 (2003).
 - [27] P. N. Pusey and W. van Meegen, *J. Chem. Phys.* **80**, 3513 (1984).
 - [28] G. C. Berry, *J. Chem. Phys.* **44**, 4550 (1966).
 - [29] P. G. Bolhuis and D. A. Kofke, *Phys. Rev. E* **54**, 634 (1996).
 - [30] P. Bartlett, *J. Chem. Phys.* **107**, 188 (1997).
 - [31] P. N. Segrè, W. van Meegen, P. N. Pusey, K. Schätzel, and W. Peters, *J. Mod. Optics* **42**, 1929 (1995).
 - [32] A. Moussaïd and P. N. Pusey, *Phys. Rev. E* **60**, 5670 (1999).
 - [33] K. N. Pham, S. U. Egelhaaf, A. Moussaïd, and P. N. Pusey, to be published.
 - [34] T. Eckert and E. Bartsch, *Faraday Discuss.* **123**, 51 (2003).
 - [35] J.-P. Bouchaud, in *Soft and Fragile Matter and Nonequilibrium Dynamics and Metastability and Flows*, edited by M. E. Cates and M. R. Evans (Institute of Physics Publishing, 2000), Scottish Universities Summer School in Physics.
 - [36] W. van Meegen, T. C. Mortensen, S. R. Williams, and J. Müller, *Phys. Rev. E* **58**, 6073 (1998).
 - [37] W. van Meegen, S. M. Underwood, and P. N. Pusey, *Phys. Rev. Lett.* **67**, 1586 (1991).
 - [38] W. Schaert and H. Sillescu, *J. Stat. Phys.* **77**, 1007 (1994).
 - [39] B. Widom, *Science* **157**, 375 (1967).
 - [40] P. N. Pusey, in *Liquids, Freezing and the Glass Transi-*

tion, edited by J.-P. Hansen, D. Levesque, and J. Zinn-Justin (Elsevier, Amsterdam, 1991), chap. 10.

[41] In our system the estimated distance between particles for samples I–K ($\phi = 0.64$) from random close pack ($\phi_{rcp} = 0.69$) is $(\phi_{rcp}/\phi)^{1/3} = 1.03 \sim 1 + \xi/3$, where the attractive potential is half of the maximum depth.

[42] Formally, a τ^{-1} distribution of decay times gives a decay linear in $\log \tau$. Limitations in our data mean, however, that we cannot use them to back out the actual decay-time distribution in our samples.

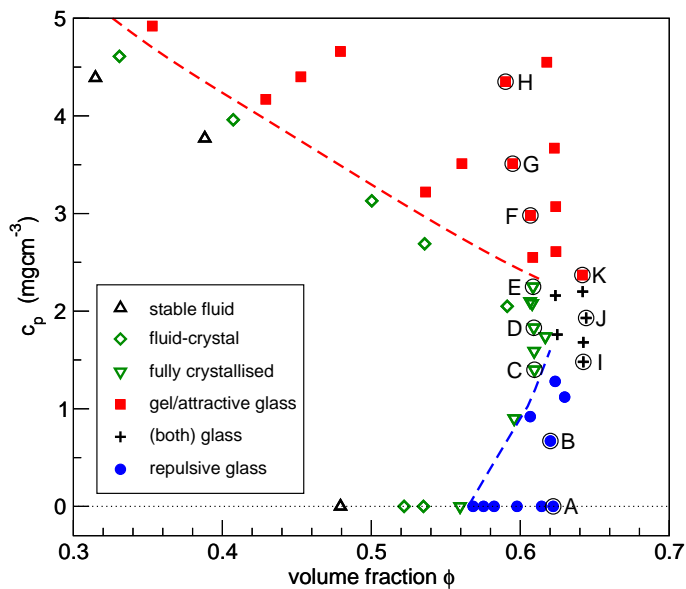


FIG. 1: Equilibrium and non-equilibrium behaviors of a colloid-polymer mixture of $\xi = 0.09$. Open symbols are those that reached thermal equilibrium (fluid, fluid-crystal coexistence, and fully crystallized). Other samples did not crystallize: some showed characteristics of hard-sphere glasses at the onset of sedimentation (filled circles), some showed those of attraction-driven glasses and gels (filled squares), and some showed both (pluses). Dashed curves are guides to the eye showing the observed boundary where crystallization ceased. Light scattering data for marked samples labeled A–K are shown in the following figures. This diagram has been shown in [24].

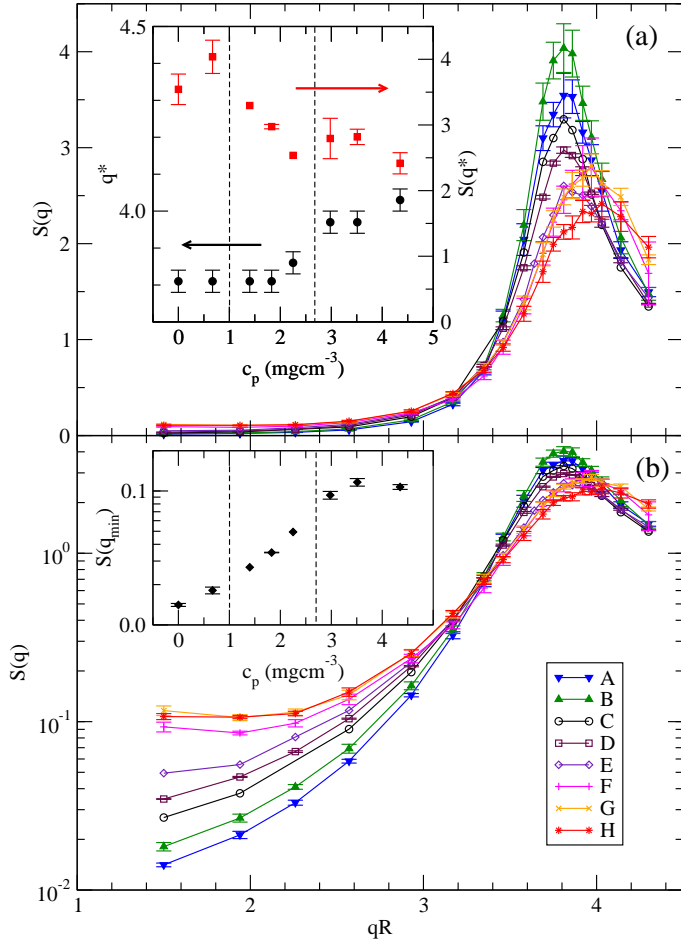


FIG. 2: Static structures factor of samples A–H ($\phi \sim 0.6$) as function of dimensionless wave vector qR . The lines are guides to the eye. (a) The peak position q^* shifts to higher q , while its height reduces and width increases upon increasing attraction. The inset shows the peak positions and heights of these static structure factors as a function of polymer concentration. (b) The same SSFs plotted with logarithmic vertical axis shows the increase of $S(q)$ at low q . The inset shows $S(q)$ at the lowest wave vector $qR = 1.50$. Vertical dashed lines in both insets indicate the glass transitions observed in Fig. 1.

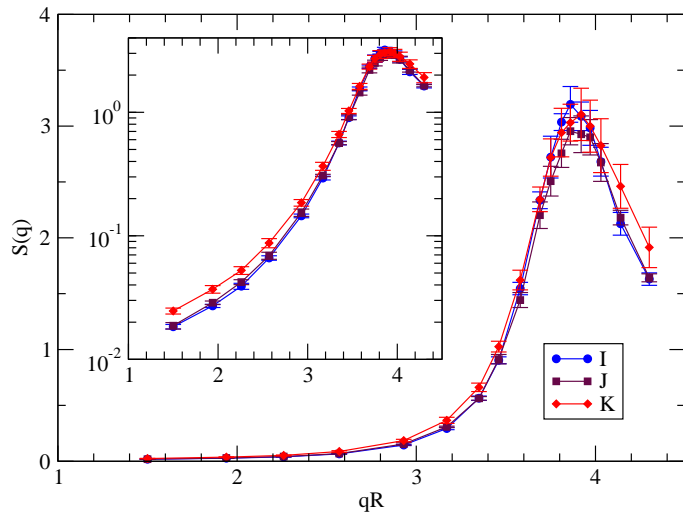


FIG. 3: Static structure factors of samples I–K with $\phi \sim 0.64$. The inset shows the same data with a logarithmic vertical axis.

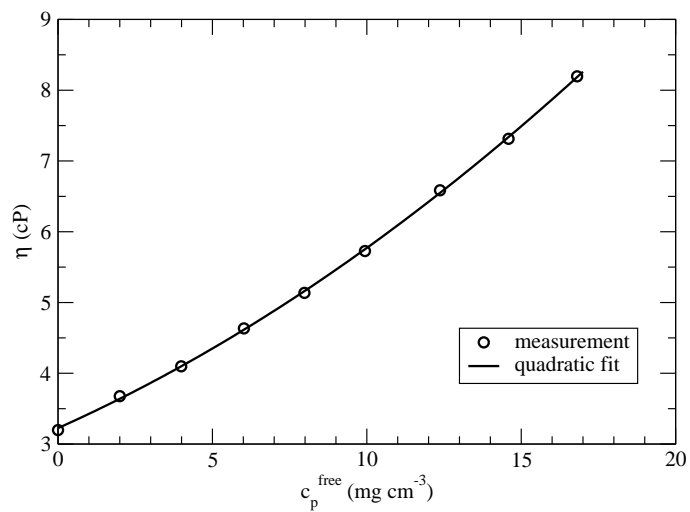


FIG. 4: The viscosity of polystyrene in *cis*-decalin at 20°C at different polymer concentrations. A quadratic fit (solid line) was used to interpolate to viscosities of samples with different c_p^{free} .

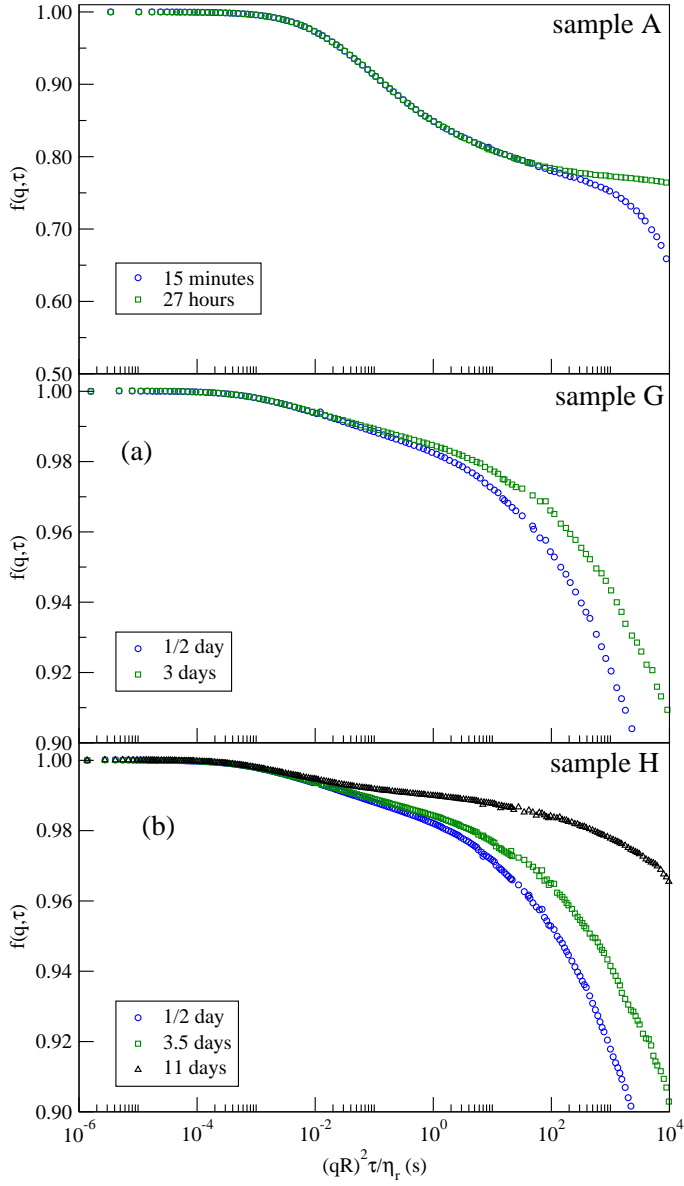


FIG. 5: Aging in samples A, G and H at $qR = 2.93$. The legend indicates the waiting time between the end of tumbling and the start of measurements. The DSFs slow down and the points of inflection become clearer with increasing age of the samples.

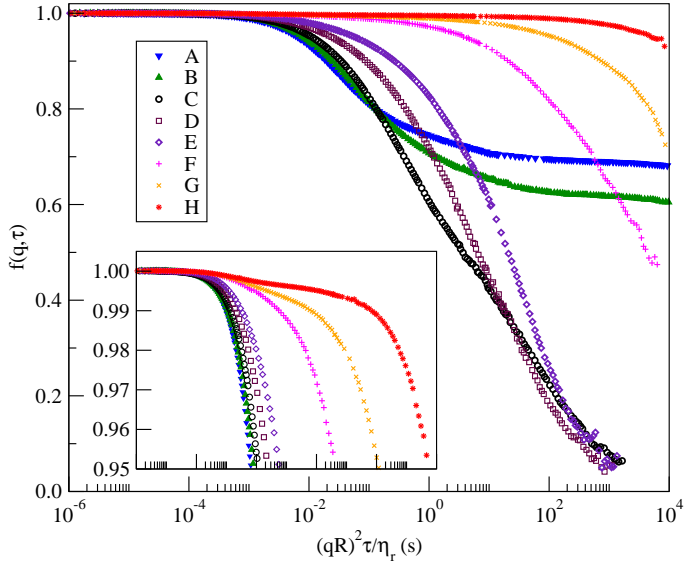


FIG. 6: Collective dynamic structure factors at $qR = 1.50$ from samples A–H spanning the re-entrant region. The time axis is scaled to dimensionless length scale $(qR)^2$ and relative polymer solution viscosity η_r . The inset shows the same plots on an expanded vertical axis.

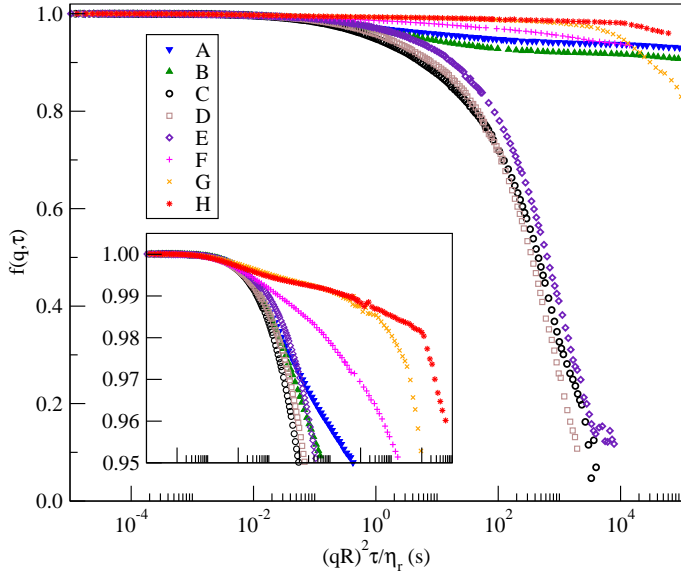


FIG. 7: DSFs at the peak of the SSFs for samples A–H. The inset shows the same plots on an expanded vertical axis.

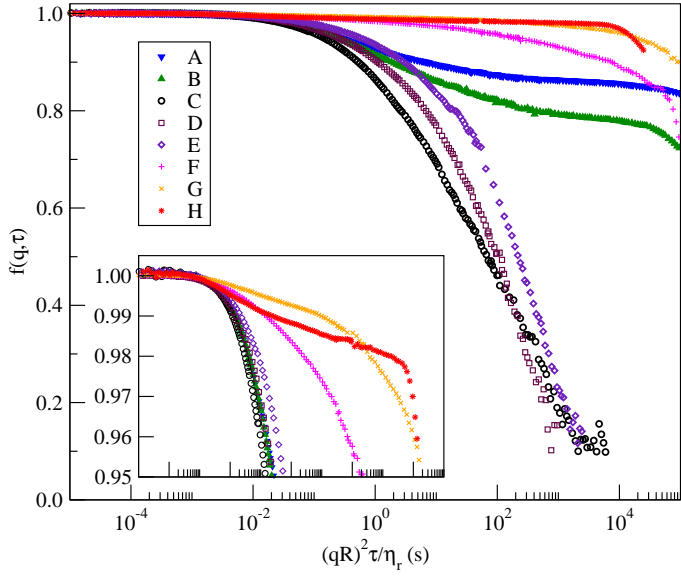


FIG. 8: DSFs of samples A-H at $qR = 4.30$, to the right of all $S(q)$ peaks. The inset shows the same plots on an expanded vertical axis.

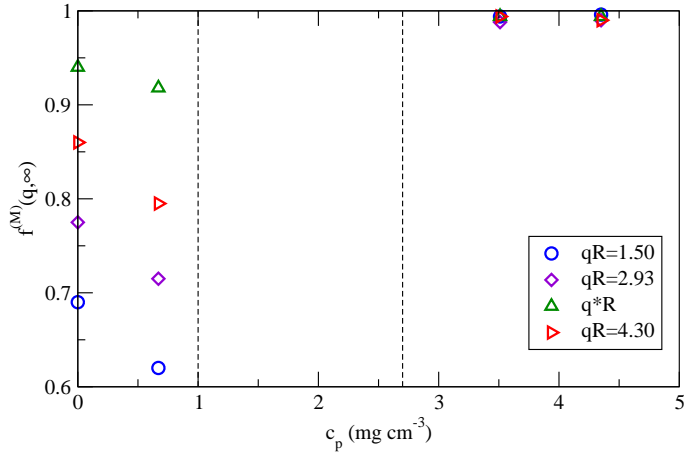


FIG. 9: The measured non-ergodicity parameters, $f^{(M)}(q, \infty)$, at different wave vectors as a function of polymer concentration in samples (left to right) A, B, G, and H. The dashed lines indicate the glass transitions observed in Fig. 1.

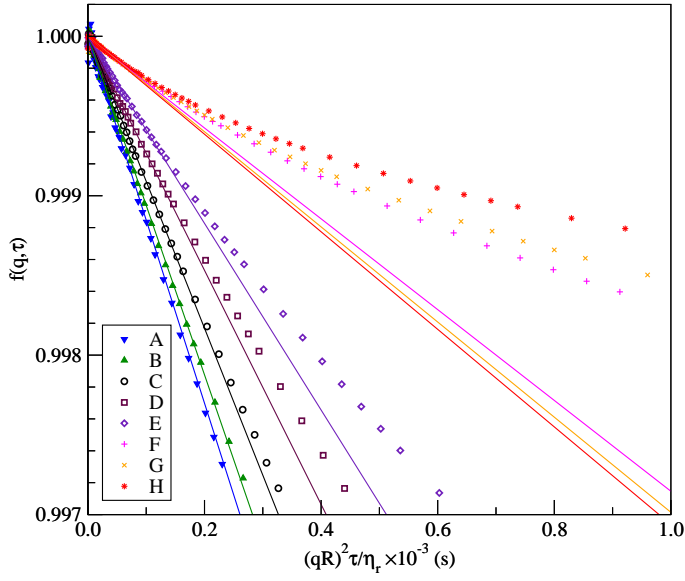


FIG. 10: The short-time dynamics of samples A–H at $qR = 1.50$. The straight lines are fits to the linear part of the DSFs at $\tau \rightarrow 0$. The dynamics departs from an initial diffusive regime progressively earlier upon increasing attraction. The short-time diffusion coefficient in the limit $\tau \rightarrow 0$ is also reduced significantly.

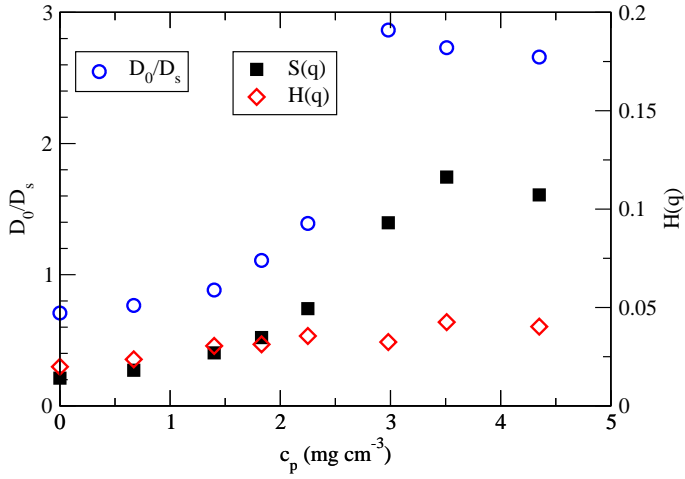


FIG. 11: The normalized short-time diffusion coefficient D_0/D_s (circles, left scale), static structure factor $S(q)$ and hydrodynamic factor $H(q)$ (right scale) at $qR = 1.50$. D_s and $S(q)$ were extracted from Fig. 10 and 2 respectively. The decrease in D_s is nearly in line with the increase in $S(q)$ so that $H(q)$ only increased slightly.

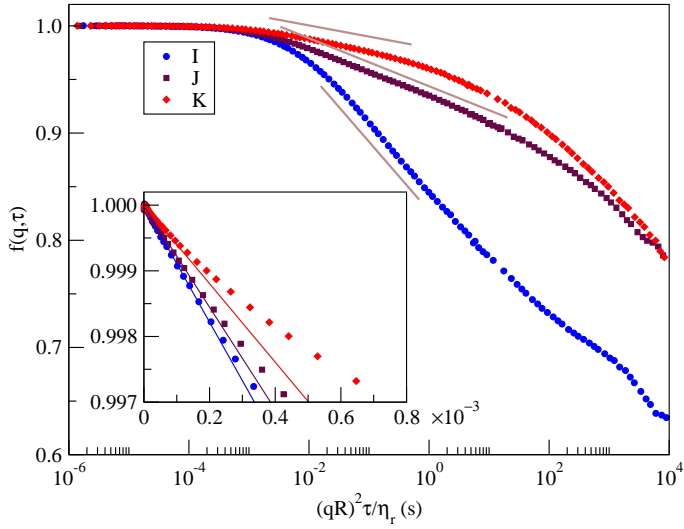


FIG. 12: The DSFs at $qR = 1.50$ for samples I–K with $\phi \sim 0.64$. Extremely stretched relaxation is found in all three samples with logarithmic decay over long ranges of τ (straight lines). The inset shows the short-time dynamics, which deviate from the diffusive regime from very early times.

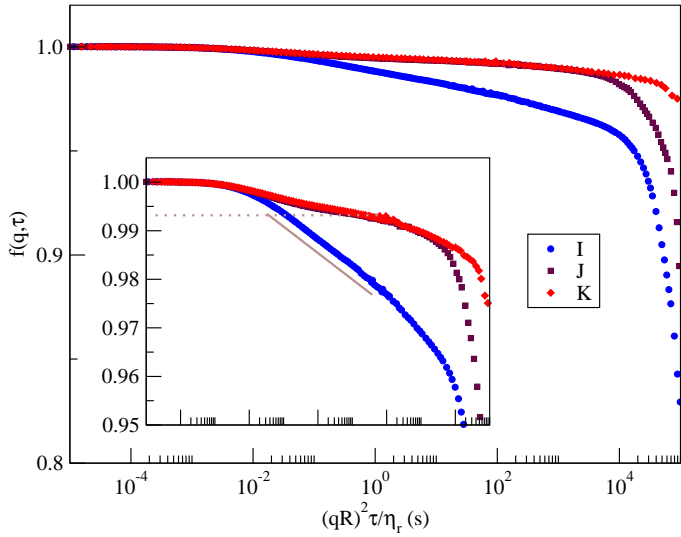


FIG. 13: DSFs at the peak of the SSH for samples I–K. All decay much slower than at low q . Sample I shows a logarithmic decay for about 3 decades in scaled time. Samples J and K develop very high plateaus (inset).

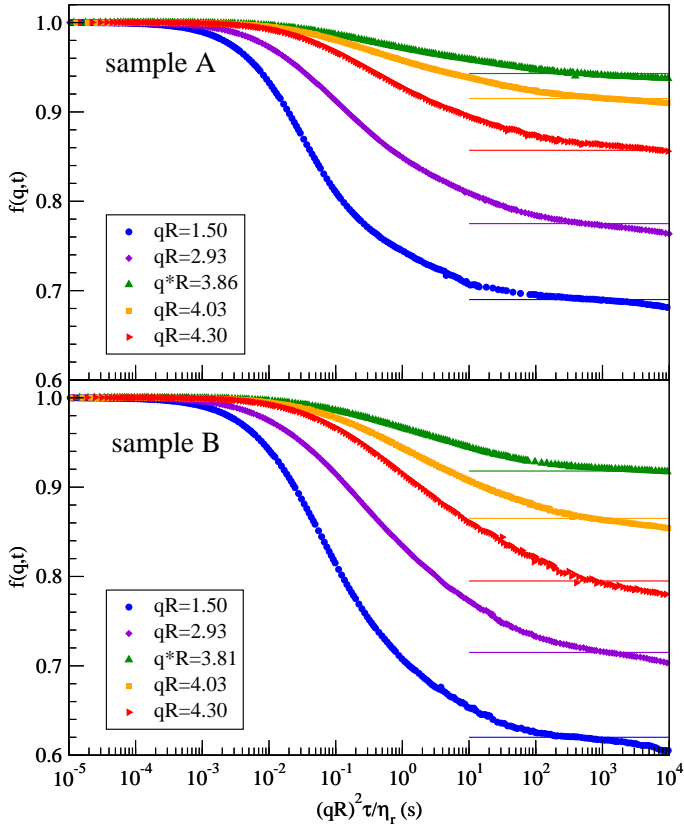


FIG. 14: The DSFs of samples A and B at different q vectors, q^* denotes the peak position of the static structure factor $S(q)$. The general shape of the DSFs are very similar. Horizontal lines denotes the height of the plateau (non-ergodicity parameters) that are plotted in Figs. 9 and 18.

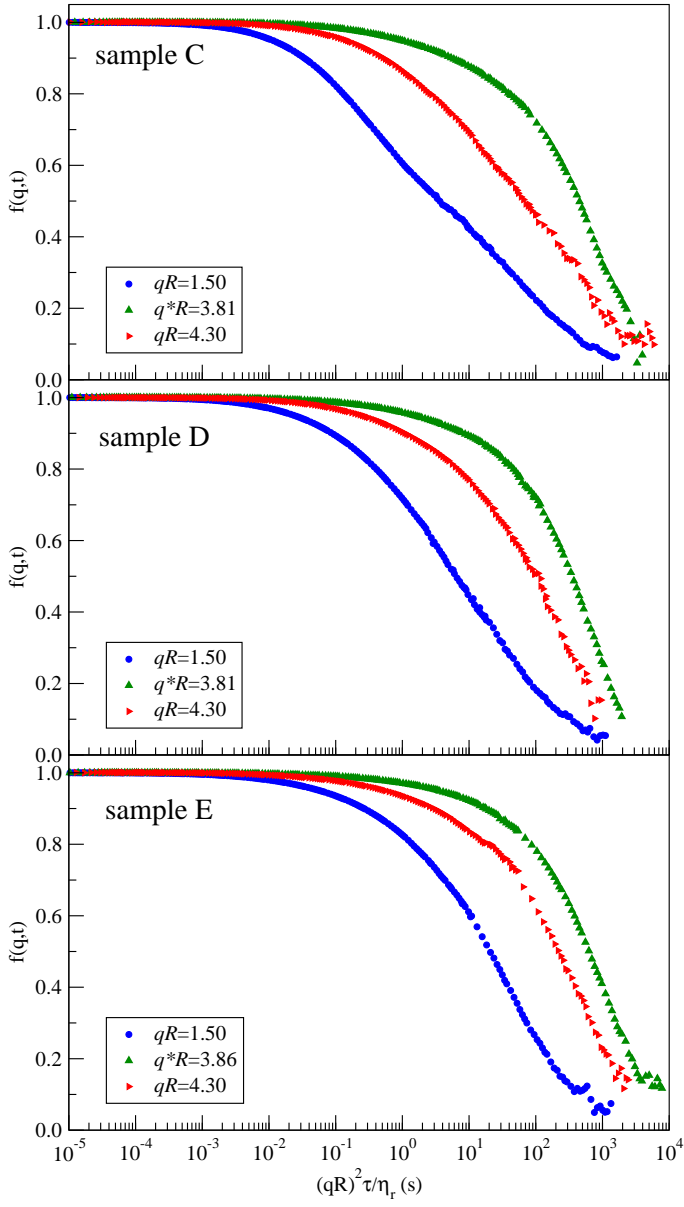


FIG. 15: The DSFs of samples C–E at different q . The rate of decay varies in the opposite direction to $S(q)$ (c.f. Fig. 2). However, all decay to zero at approximately the same scaled time. Except for sample C at the lowest q , all other DSFs do not show two distinct relaxation processes as other dense fluids.

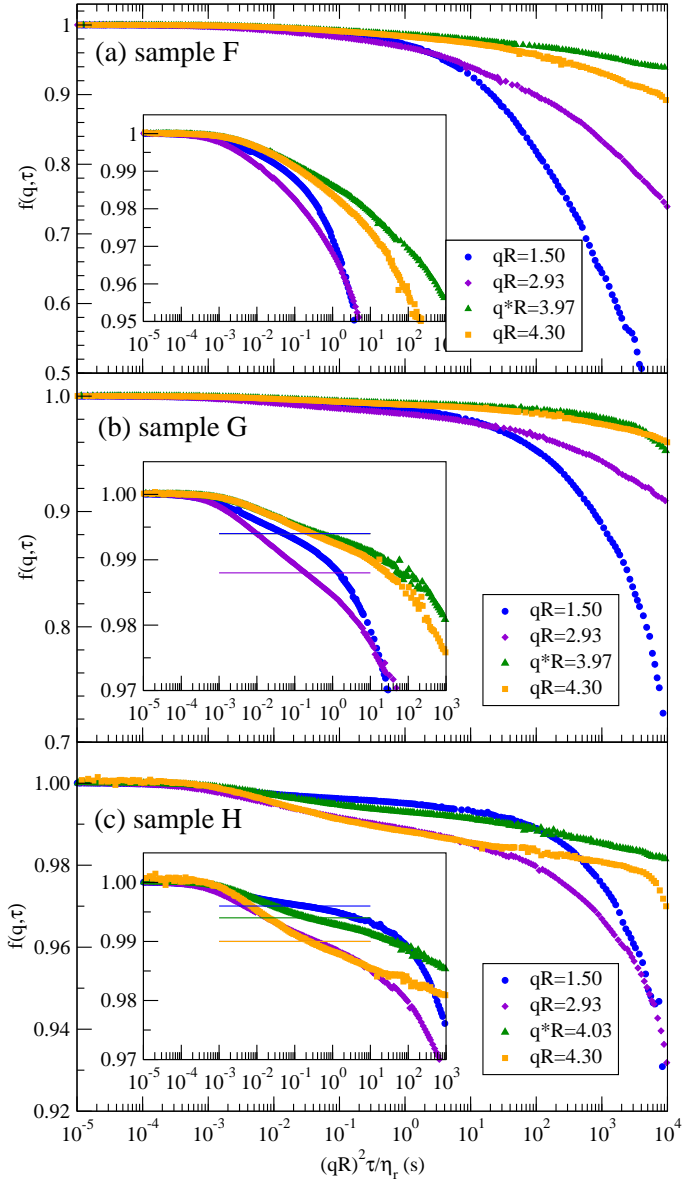


FIG. 16: The DSFs of samples F–H at different q . The vertical axes span different ranges. Sample F did not show a point of inflection, but G and H have very high points of inflection (horizontal lines), the values of which are used in Figs. 9 and 18.

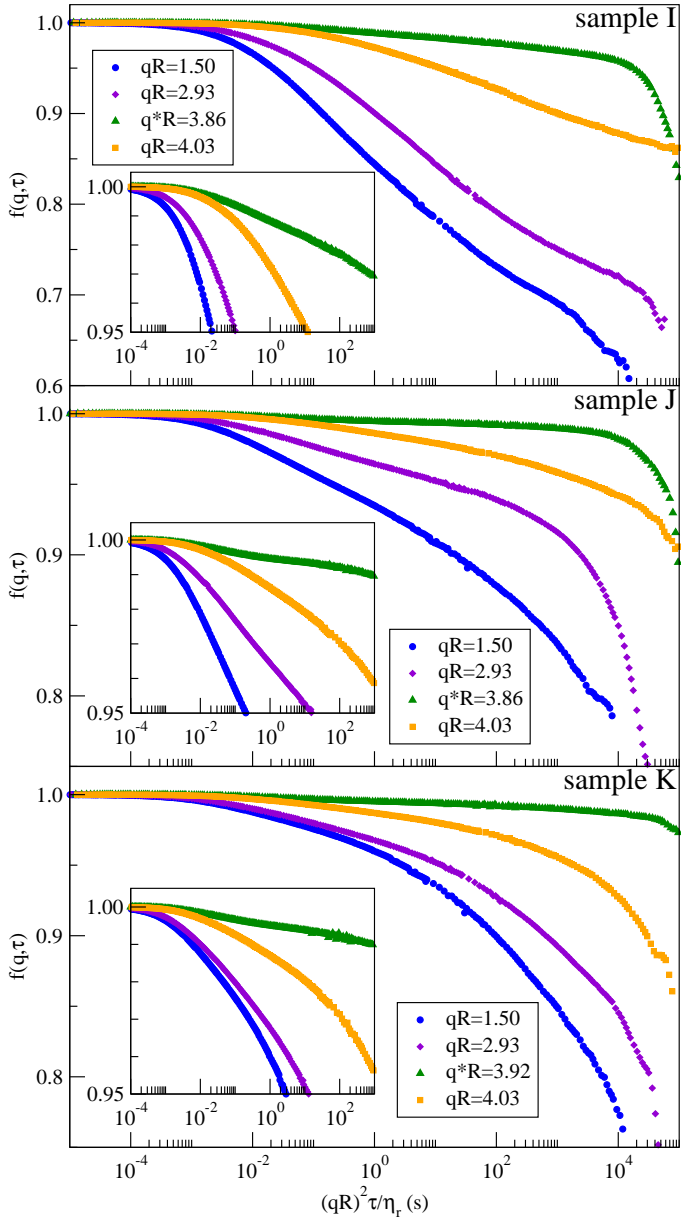


FIG. 17: The DSFs of samples I, J and K at different q . The insets show the same quantities with expanded vertical axes. The relaxations show similar behavior at all wave vectors except at the peak of $S(q)$. Sample I decays to a logarithmic section and then appears to turn up to a plateau. Sample J shows a very long section of logarithmic decay. Sample K is similar to J with a shorter stretch of logarithmic decay. In the early decay at the peak of $S(q)$, the DSF of sample I has a long stretch of logarithmic decay whereas samples J and K develop very high plateaus.

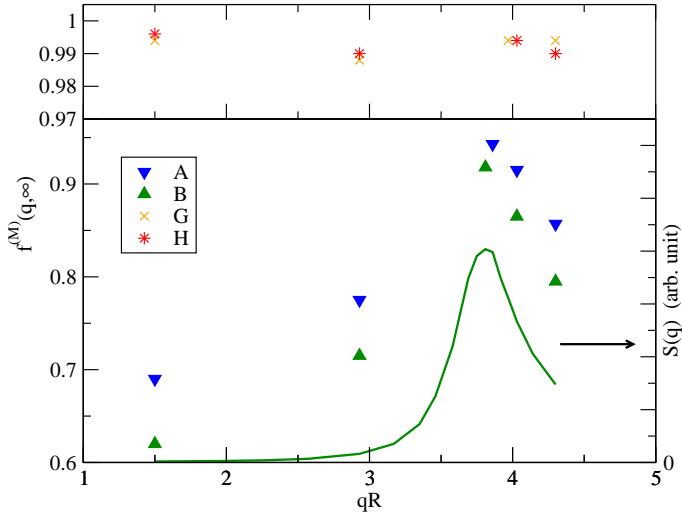


FIG. 18: The measured non-ergodicity parameters of samples A, B, G and H as a function of scattering vector q (points), and the static structure factor of sample B (line) for comparison. The non-ergodicity parameters of repulsive glasses A and B follow the static structure factor, whereas those of the attractive glass are extremely high and hardly fluctuate with q (upper pane with expanded vertical axis).